

Molecular dynamics study of primary radiation damage in TiVTa concentrated solid-solution alloy

Yong-Peng Zhao(赵永鹏), Yan-Kun Dou(豆艳坤), Xin-Fu He(贺新福), Han Cao(曹晗), Lin-Feng Wang(王林枫), Hui-Qiu Deng(邓辉球), and Wen Yang(杨文)

Citation: Chin. Phys. B, 2024, 33 (**3**): 036104. DOI: 10.1088/1674-1056/ad0146
Journal homepage: http://cpb.iphy.ac.cn; http://iopscience.iop.org/cpb

What follows is a list of articles you may be interested in

Anelasticity to plasticity transition in a model two-dimensional amorphous solid

Baoshuang Shang(尚宝双)
Chin. Phys. B, 2024, 33 (**1**): 016102. DOI: 10.1088/1674-1056/acf82c

Universal basis underlying temperature, pressure and size induced dynamical evolution in metallic glass-forming liquids

H P Zhang(张华平), B B Fan(范蓓蓓), J Q Wu(吴佳琦), and M Z Li(李茂枝)
Chin. Phys. B, 2024, 33 (**1**): 016101. DOI: 10.1088/1674-1056/acf994

Classification and structural characteristics of amorphous materials based on interpretable deep learning

Jiamei Cui(崔佳梅), Yunjie Li(李韵洁), Cai Zhao(赵偲), and Wen Zheng(郑文)
Chin. Phys. B, 2023, 32 (**9**): 096101. DOI: 10.1088/1674-1056/acd7d0

Influence of temperature and alloying elements on the threshold displacement energies in concentrated Ni-Fe-Cr alloys

Shijun Zhao(赵仕俊)
Chin. Phys. B, 2021, 30 (**5**): 056111. DOI: 10.1088/1674-1056/abf10d

Understanding defect production in an hcp Zr crystal upon irradiation: An energy landscape perspective

Jiting Tian(田继挺)
Chin. Phys. B, 2021, 30 (**2**): 026102. DOI: 10.1088/1674-1056/abbbe0

Molecular dynamics study of primary radiation damage in TiVTa concentrated solid-solution alloy

Yong-Peng Zhao(赵永鹏)[1], Yan-Kun Dou(豆艳坤)[1,†], Xin-Fu He(贺新福)[1,‡], Han Cao(曹晗)[1], Lin-Feng Wang(王林枫)[1], Hui-Qiu Deng(邓辉球)[2], and Wen Yang(杨文)[1]

[1] *Reactor Engineering Technology Research Division, China Institute of Atomic Energy, Beijing* 102413, *China*
[2] *School of Physics and Electronics, Hunan University, Changsha* 410082, *China*

(Received 28 July 2023; revised manuscript received 22 September 2023; accepted manuscript online 9 October 2023)

The primary radiation damage in pure V and TiVTa concentrated solid-solution alloy (CSA) was studied using a molecular dynamics method. We have performed displacement cascade simulations to explore the generation and evolution behavior of irradiation defects. The results demonstrate that the defect accumulation and agglomeration in TiVTa CSA are significantly suppressed compared to pure V. The peak value of Frenkel pairs during cascade collisions in TiVTa CSA is much higher than that in pure V due to the lower formation energy of point defects. Meanwhile, the longer lifetime of the thermal spike relaxation and slow energy dissipation capability of TiVTa CSA can facilitate the recombination of point defects. The defect agglomeration rate in TiVTa CSA is much lower due to the lower binding energy of interstitial clusters and reduced interstitial diffusivity. Furthermore, the occurrence probability of dislocation loops in TiVTa CSA is lower than that in pure V. The reduction in primary radiation damage may enhance the radiation resistance of TiVTa CSA, and the improved radiation tolerance is primarily attributed to the relaxation stage and long-term defect evolution rather than the ballistic stage. These results can provide fundamental insights into irradiation-induced defects evolution in refractory CSAs.

Keywords: concentrated solid-solution alloy, primary radiation damage, molecular dynamics simulation

PACS: 61.72.J–, 02.70.Ns, 61.82.Bg **DOI:** 10.1088/1674-1056/ad0146

1. Introduction

Concentrated solid-solution alloys (CSAs) have been reported to exhibit outstanding properties, such as good mechanical properties, radiation tolerance and corrosion resistance, and are expected to be promising candidates to satisfy the critical requirements for extreme service environments in advanced reactor applications.[1–5] The body-centered cubic (bcc) CSAs composed of refractory elements, such as Ti, V, Ta, Nb, Zr, and Hf, have shown good physical properties due to the characteristics of the constituent elements and core effects, namely, high entropy, severe lattice distortion, sluggish diffusion and cocktail effects.[6–8] Recently, the various properties of low-activation TiVTa series refractory CSAs have been investigated, which have exhibited good thermal stability,[9–11] mechanical properties[12–16] and irradiation resistance.[17,18] It has been preliminary demonstrated that the irradiation-induced defect clusters and irradiation hardening are suppressed in TiVTa CSA.[18] However, the underlying mechanism of radiation damage in TiVTa CSA is still not clear, and there is an urgent need for specialized research.

Neutrons or ions can transport part of their energy to atoms, resulting in the creation of a primary knock-on atom (PKA) during irradiation.[19] Then, cascade collisions are provoked and a large number of Frenkel pairs (FPs) are produced. These point defects can move through the material and diffuse and cluster at different locations, leading to the formation of extended defects, such as voids, stacking fault tetrahedra or dislocation loops.[20] In the long-term, the evolution of irradiation defects can result in the long-range irradiation-induced damage phenomena, such as irradiation swelling, radiation-induced segregation and precipitation, which can affect the mechanical properties of materials. Therefore, the generation, distribution and evolution of defects during displacement cascades play an important role in revealing the mechanism of irradiation resistance in TiVTa CSA.

Molecular dynamics (MD) is a powerful methodology that is used to investigate the generation and evolution behavior of irradiation-induced defects in both conventional metals and CSAs.[19–28] Multiple studies have shown that CSAs possess radiation damage resistance, which mainly originate from the alteration of defect formation energies and migration dynamics.[21,22] In Ni-based CSAs with face-centered cubic (fcc) structures, the suppressed damage accumulation and evolution caused by a higher defect recombination rate during cascade collision simulations were observed compared to pure Ni, which can be explained by the reduced thermal conductivity and enhanced thermal spike.[23–25] Furthermore, Ni-based CSAs have shown better radiation resistance due to the reduction of interstitial mobility with increased alloy complexity.[26–29] Meanwhile, in Mo-based refractory CSAs,

†Corresponding author. E-mail: douyankun@cnncmail.cn
‡Corresponding author. E-mail: hexinfu@cnncmail.cn

© 2024 Chinese Physical Society and IOP Publishing Ltd

more principal elements may not result in better radiation resistance from the perspective of the displacement cascade process.[30] Based on Frenkel pair accumulation simulations, it is concluded that the clustering behavior of defects in bcc TiVTa and VTaW CSAs can be affected by the chemical fluctuations, leading to small defect clusters or even discrete point defects.[22] In MoNbTiV-based bcc CSAs, only dislocation loops were formed after helium ion irradiation, while no voids or precipitates were observed, thus showing good irradiation resistance.[31] In TiVTa CSA under He ion irradiation, the irradiation-induced segregation is weak.[17] In addition, the suppressed aggregation of irradiation-induced defect clusters is observed in TiVTa CSA under Ti ion irradiation. Here, dislocation loops are the main contributors to irradiation-induced hardening, and the density and size of dislocation loops are both smaller than those of pure V, showing good resistance to defect production and growth,[18] while the underlying mechanism has not yet been ascertained. Dislocation loops are usually observed as a result of the migration and agglomeration of interstitial atoms or vacancies.[32,33] Therefore, the formation and diffusion of point defects can affect the behavior of primary damage under radiation. The peculiar point-defect properties originating from the chemical complexity and lattice disorder in TiVTa CSA have been studied recently in our reported results.[34,35] It is found that defect formation and migration energies exhibit broad distributions, sluggish defect diffusion was observed compared to pure V. However, the generation and evolution behavior of irradiation defects in TiVTa CSA still remain unclear; a detailed study on the primary radiation damage is needed to further investigate the irradiation performance of TiVTa CSA.

In this work, primary radiation damage simulations in pure V and TiVTa CSA were performed using the molecular dynamics method. Displacement cascades were carried out and the evolution behavior of irradiation-induced defects was analyzed, including Frenkel pairs, defect clusters and dislocation loops. The remainder of this paper is divided into the following parts. In Section 2, the computational methods are described. Section 3 presents and discusses our simulated results of the generation and evolution behavior of defects in pure V and TiVTa CSA. Finally, a summary is given in Section 4.

2. Methodology

The cascade collision simulations were performed using the large-scale atomic/molecular massively parallel simulator (LAMMPS).[36] The Ti–V–Ta interatomic potential[37] based on the Finnis–Sinclair formalism was used, which is suitable for atomistic simulations of defects production and evolution behavior. PKA energies of 10 keV, 20 keV, and 40 keV were applied. To guarantee the cascade included in the system, the box size was set to $150a_0 \times 150a_0 \times 150a_0$, and the lattice parameter a_0 for pure V and equi-atomic TiVTa CSA was 3.037 Å and 3.214 Å, respectively. The simulated configurations were derived by altering the distribution of elements while keeping the concentration constant. Once the cascade collision exceeded the boundary of the simulation box, the simulation results were discarded; 30 simulations were performed for each case. Periodic boundary conditions were employed along all directions.

The system was initially relaxed to an energy minimization using a conjugate gradient method, followed by a 25 ps relaxation under an isothermal–isobaric ensemble (NPT) at 300 K. An atom near the center of the system was selected as a PKA. Then, the displacement cascade process was conducted in the microcanonical ensemble (NVE) with a variable timestep. To ensure full annealing of cascading collisions, all simulations were carried out with a total of 100 ps. The atomic position information was output at different moments for analysis.

The Open Visualization tool and its included tools[38–41] were used to visualize and analyze the evolution behavior of defects. The formed Frenkel pairs were identified using Wigner–Seitz defect analysis. The cluster analysis tool was used to define the defect clusters, where the cut-off radius is the second-nearest-neighbor distance and third-nearest-neighbor distance for vacancy and interstitial clusters, respectively. The formed dislocation loops were analyzed using the implemented dislocation extraction algorithm (DXA). Structure analysis was carried out using polyhedral template matching (PTM), with the root-mean-square deviation (RMSD) equal to 0.2.

To better understand the interstitial clustering behavior, the binding energies of interstitial clusters of different sizes were calculated. The binding energy of an interstitial cluster with n interstitials, $E_{\mathrm{b}}^{i_1,i_2,\ldots,i_n}$, can be calculated using

$$E_{\mathrm{b}}^{i_1,i_2,\ldots,i_n} = \sum_{j=1}^{n} E_{\mathrm{f}}^{i_j} - E_{\mathrm{f}}^{i_1,i_2,\ldots i_n}, \tag{1}$$

$$E_{\mathrm{f}}^{i_1,i_2,\ldots,i_n} = E_{N+n} - \frac{N+n}{N} E_N, \tag{2}$$

where $E_{\mathrm{f}}^{i_j}$ is the formation energy of a single interstitial defect j, and $E_{\mathrm{f}}^{i_1,i_2,\ldots,i_n}$ is the formation energy of an interstitial cluster with n interstitials.[23,42] Here, $E_{\mathrm{f}}^{i_1,i_2,\ldots,i_n}$ can be calculated using formula (2), where E_{N+n} and E_N are the energies of supercells with and without n interstitials, and N is the total number of atoms.

3. Results and discussion

3.1. Frenkel pairs

First, the generation and recombination behavior of point defects were studied. The evolution of the number of Frenkel

Pairs generated during cascade collision simulations with three different PKA energies is plotted in Fig. 1. After the introduction of PKA, FPs are generated continuously during cascade collisions and the number of FPs rises rapidly to the peak. This process can last approximately 0.3 ps to 2 ps, depending on both the type of simulated material and the PKA energy. When the number of point defects reaches its peak, it starts to decrease due to the recombination of vacancies and interstitials during the relaxation of the thermal spike, and finally reaches a stable value after about 5 ps to 20 ps. The relaxation of the thermal spike can be defined as the period starting from the moment when the maximum number of FPs is reached and extends to the subsequent stable stage.[23] Taking the cascade collision simulations with a PKA of 10 keV as an example, the peak damage occurs at 0.35 ps and 1 ps for pure V and TiVTa CSA, respectively. The number of point defects in pure V is found to reach a steady state after 5 ps, while it requires approximately 10 ps in TiVTa CSA, suggesting a longer recombination time of point defects in the latter. The thermal conductivity of pure V is 35 $W{\cdot}m^{-1}{\cdot}K^{-1}$ at room temperature,[43] and it is 20 $W{\cdot}m^{-1}{\cdot}K^{-1}$ in TiVTa CSA tested by our team. The lower thermal conductivity can retard the heat dissipation of the cascade core in TiVTa CSA, which is believed to account for the longer lifetime of the relaxation of the thermal spike and the higher defect recombination efficiency.[23] Compared with pure V, the number of peak defects in TiVTa CSA is much higher, which can be explained by the lower formation energies of the point defects reported in our previous results.[34,35] Although TiVTa CSA has longer time for defect recombination, the average number of surviving defects in TiVTa CSA is still a little higher than that in pure V.

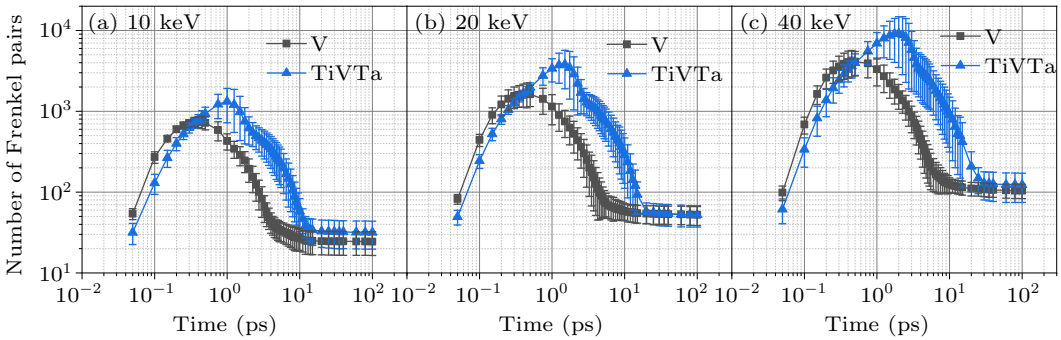


Fig. 1. The average number of Frenkel pairs versus time for cascade collision simulations with different PKA energies (10 keV, 20 keV, 40 keV) for pure V (black squares) and TiVTa CSA (blue triangles). The error bars indicate the standard deviation after averaging over all cascades for each case.

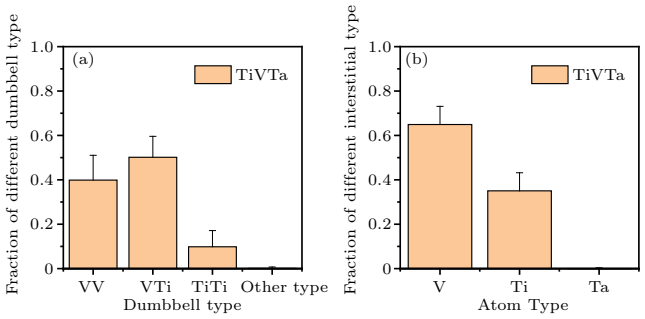


Fig. 2. The fraction of different (a) dumbbell-type and (b) atom-type interstitials in the 10 keV cascade collision simulations in TiVTa CSA.

Based on the 10 keV cascade collision simulations, the statistics of surviving interstitial types in TiVTa CSA are obtained in Fig. 2. It is found that interstitials exist mostly in the form of VV, VTi and TiTi dumbbells, which agrees with the results of defect formation energies gained by first-principles calculations in our previous studies.[34,35] In TiVTa CSA, VV and VTi dumbbells have lower formation energies of 1.50 ± 0.21 eV and 1.83 ± 0.23 eV, respectively. TiTi dumbbell formation energies are a little higher at 2.25 ± 0.23 eV. Dumbbells containing Ta atoms are the most difficult to form with the highest formation energies. Since V atoms have a smaller atomic radius than Ti and Ta atoms,[44] they are much more inclined to exhibit as interstitials. Furthermore, Ti atoms have positive binding energy with V atoms, while Ta atoms are repulsive to V atoms.[37] Therefore, VV and VTi dumbbells are the most stable configurations in TiVTa CSA. The formation energy of point defects can affect the evolution of clusters and help to understand the behavior of irradiation defects over a longer time scale.

3.2. Defect clusters

Within a displacement cascade, small vacancies and interstitial clusters can form via defect aggregation. Figure 3 illustrates the number of interstitial and vacancy clusters in the stable configurations, which are counted and classified according to the cluster size. It has been demonstrated that vacancies tend to be more concentrated in pure V, while interstitials generally remain in a single interstitial state. The clustered fraction of vacancies is much higher than that of interstitials. Moreover, the occurrence probability of large-sized vacancy clusters is higher than interstitial clusters. As shown in Figs. 4(a) and 4(b), the agglomeration rates of vacancies and interstitials in TiVTa CSA are both lower than those of pure V. And there is no significant difference between the clustered fractions of vacancies and interstitials in TiVTa

CSA. The PKA energy has little influence on the clustered defects fraction within the range of 10 keV to 40 keV. Moreover, TiVTa CSA has fewer large-sized defect clusters than pure V. The number of defect clusters decreases as the cluster size increases.

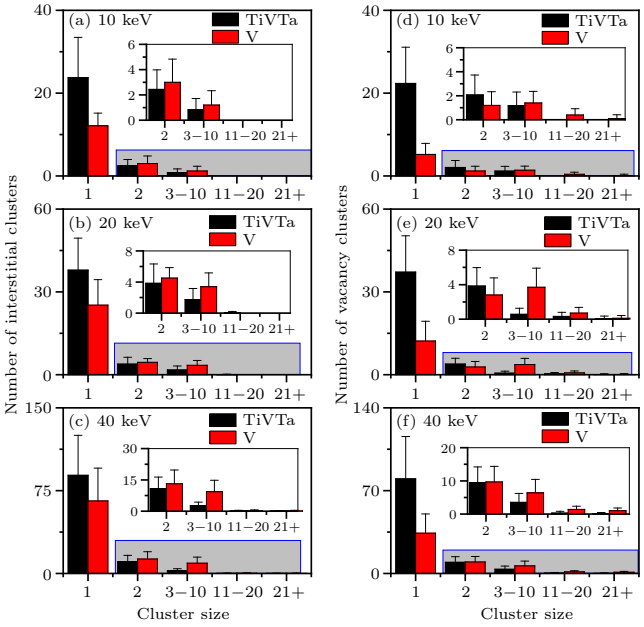


Fig. 3. The average number of different sized (a)–(c) interstitial clusters and (d)–(f) vacancy clusters in pure V and TiVTa CSA after cascade collision simulations with different PKA energies.

It is indicated that the formation energies of interstitials and the binding energies of interstitial clusters can help one to judge the performance of defect evolution behavior.[42] As shown in Fig. 4(c), it can be concluded that TiVTa CSA has the lowest interstitial-cluster binding energies due to compositional heterogeneity[30] compared to pure V, which means fewer clusters can form and survive. Furthermore, there is much more difference in the diffusion behavior of interstitials between pure V and TiVTa CSA, the diffusion of interstitials in TiVTa CSA is severely suppressed.[35] The reduced interstitial diffusivity in TiVTa CSA is believed to contribute to the suppressed clustering of defects. Due to the severe lattice distortions caused by the random arrangement of multiple constituent elements, the diffusion of interstitials in TiVTa CSA is hindered and the migration barrier is much higher than that of pure V.[35] Meanwhile, interstitials in TiVTa CSA exhibit three-dimensional diffusion, while interstitials diffuse one-dimensionally in pure V when the temperature is lower than 600 K.[45] It is concluded that the clustering behavior of defects in bcc TiVTa CSA can be affected by the chemical fluctuations, leading to small defect clusters or even discrete point defects. The accumulation of point defects is suppressed in TiVTa CSA, which can improve the difficulty of the formation of large-sized defect clusters. Although the number of surviving point defects generated by cascade collisions in TiVTa CSA is relatively higher than pure V, the defect agglomeration rate is much lower. This is due to the lower binding energy of interstitial clusters and sluggish diffusion of interstitials, leading to fewer defect clusters and better resistance to defect growth.

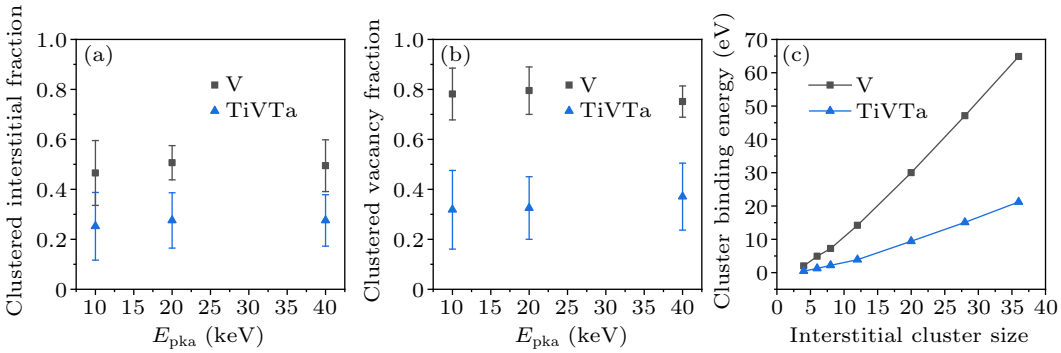


Fig. 4. (a)–(b) Clustered defect fractions of cascade simulations with different PKA energies. (c) The binding energy of interstitial clusters in pure V and TiVTa CSA.

3.3. Dislocation loops

Dislocation loops are generally irradiation-induced defects in bcc metals, which are the dominant contributions to irradiation hardening in pure V and TiVTa CSA.[18] As shown in Table 1, the number of different types of dislocation loops created under different conditions is counted. No dislocation loops can be observed at the PKA energy of 10 keV, which is consistent with the few defect clusters. The formation of dislocation is predominated by the clustering of vacancies or interstitial atoms. The occurrence probability of large clusters improves with the increase in PKA energy. When the PKA energy increases to 20 keV, $(1/2)\langle 111\rangle$ interstitial and vacancy loops appear in many cases of pure V. Due to the lower defect agglomeration rate in TiVTa CSA, fewer dislocation loops are created during cascade collisions than in pure V, and the size of the dislocation loops is smaller. Compared with pure V, dislocation loops are more difficult to form in TiVTa CSA. When the PKA energy equals 40 keV, $(1/2)\langle 111\rangle$ dislocation loops are found in both pure V and TiVTa CSA. Here, $\langle 100\rangle$ interstitial and vacancy dislocation loops are observed in pure V, while only $\langle 100\rangle$ vacancy loops can be seen in TiVTa CSA among all the 40 keV simulations. It is indicated that the re-

duction in primary radiation damage may contribute to the irradiation resistance in TiVTa CSA. In addition, for pure V, point defects are more likely to form dislocation loops with Burgers vectors of $(1/2)\langle 111\rangle$ rather than $\langle 100\rangle$, which is consistent with the calculated formation energies of dislocation loops,[46] while the formation preference of dislocation loops cannot be determined in TiVTa CSA.

Table 1. The counts of different types of dislocation loops in pure V and TiVTa CSA, statistically based on 30 cascade simulations for each condition.

E_{pka} (keV)	Metal	$(1/2)\langle 111\rangle$ interstitial loops	$\langle 100\rangle$ interstitial loops	$(1/2)\langle 111\rangle$ vacancy loops	$\langle 100\rangle$ vacancy loops
10	V	0	0	0	0
	TiVTa	0	0	0	0
20	V	4	0	8	0
	TiVTa	1	0	0	0
40	V	4	1	10	1
	TiVTa	3	0	0	1

After cascade collisions, a few dislocation loops were observed in TiVTa CSA, including $(1/2)\langle 111\rangle$ interstitial dislocation loops and $\langle 100\rangle$ vacancy dislocation loops. In Fig. 5, the typical morphologies of peak damage and the surviving defects for 40 keV cascades in TiVTa CSA are displayed: (a1)–(d1) for the $\langle 100\rangle$ vacancy dislocation loop, and (a2)–(d2) for the $(1/2)\langle 111\rangle$ interstitial dislocation loop, respectively. In Fig. 5(a1), it can be seen that sub-cascades can occur when the PKA energy is high enough, while in Fig. 5(a2) the cascade core is compact. Figures 5(b1) and 5(b2) show the final configurations, containing mostly point defects. The discrete distributions of point defects are demonstrated in Figs. 5(c1) and 5(c2); isolated defects and small clusters with the separation of vacancies from interstitials can be seen intuitively. Vacancies are distributed in the core of the cascade collision, while interstitials are scattered around them, which is mainly caused by the easier diffusion for interstitials than vacancies. Moreover, figures 5(d1) and 5(d2) illustrate two typical structures of dislocation loops in TiVTa CSA, namely, the $\langle 100\rangle$ vacancy dislocation loop and the $(1/2)\langle 111\rangle$ interstitial dislocation loop, with the latter mainly consisting of V and Ti atoms. Recently, the microstructure induced by Ti ion irradiation at room temperature in TiVTa CSA has been investigated.[18] No irradiation-induced precipitation was observed, and the elemental clustering was insignificant. Moreover, the average size and density of dislocation loops in TiVTa CSA were both smaller than in pure V, and loop rafting was only observed in pure V. It is found that the simulation results of cascade collisions agree with the experimental phenomenon, and the size and number of defect clusters in TiVTa CSA are much lower than those in pure V.[18] It should be noted that the displacement cascades occur within a short period, much shorter than the experimental time scale. Therefore, the direct comparison of dislocation loops between simulations and experiments is inappropriate. It is necessary to simulate the evolution behavior of defects over a longer time scale using other methods, such as the kinetic Monte Carlo method or the cluster dynamics method. However, the displacement cascades simulation results can still qualitatively explain relevant phenomena. The simulation results show that the generated Frenkel pairs in TiVTa CSA are higher than those in pure V, while the defect agglomeration rate is much lower, leading to fewer irradiation-induced clusters or dislocation loops. By analyzing the difference in the production and evolution of irradiation defects, it is concluded that the improved radiation tolerance in TiVTa CSA is primarily attributed to the thermalization of the collisions rather than the ballistic atom collision processes.

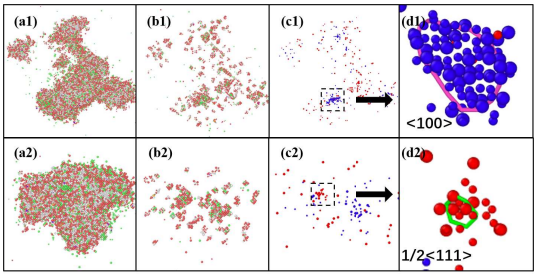


Fig. 5. Representative snapshots of defect distribution for 40 keV cascades in TiVTa CSA. (a1) and (a2) The atom structure when close to the peak damage state. (b1) and (b2) The final defect configurations. Structure types are given by PTM. Atoms are colored according to their structures: hexagonal close-packed (red), fcc (green), and unknown (white); all bcc atoms have been removed. (c1) and (c2) The distribution of FPs; the red and blue atoms represent interstitials and vacancies, respectively. (d1) and (d2) The $\langle 100\rangle$ and $(1/2)\langle 111\rangle$ dislocations identified by DXA.

In addition, it has been observed that, in comparison with pure V, dislocation loops with Burgers vectors of $\langle 100\rangle$ are the predominant defects after ion irradiation. This is not in contradiction with the theoretical simulations of cascade collisions, where both $\langle 100\rangle$ and $(1/2)\langle 111\rangle$ dislocation loops have been observed. It is believed that the prevalence of $\langle 100\rangle$ loops in TiVTa CSA may be ascribed to further defect development or specific loop reactions, which require further investigation. In α-Fe, the formation mechanism of $\langle 100\rangle$ dislocation loops has been studied widely. Riding the supersonic shockwave generated in the cascade collision, interstitials can be punched out to form $\langle 100\rangle$ dislocation loops in a few picoseconds.[47] In future, we can carry out similar cascade collision simulations with higher PKA energies and larger boxes to study the probable existing mechanism in TiVTa CSA.

4. Conclusion

In the present study, primary radiation damage has been investigated systemically in pure V and TiVTa CSA via molecular dynamics simulations. Displacement cascade simulations were carried out to study the generation and evolution behavior of irradiation defects. The following conclusions can be obtained.

(i) TiVTa CSA exhibits a substantially long lifetime of thermal spike relaxation and possesses slow energy dissipation ability due to low thermal conductivity, which can enhance the recombination of point defects.

(ii) The defect agglomeration rate in TiVTa CSA is much lower than that in pure V due to the smaller binding energy of interstitial clusters and reduced interstitial diffusivity, fewer defect clusters can form during cascade collisions.

(iii) Compared to pure V, it is more difficult to form dislocation loops in TiVTa CSA. The reduction in primary radiation damage in cascade simulations may contribute to the irradiation resistance of TiVTa CSA, and the improved radiation tolerance is primarily attributed to the thermalization of the collisions and long-term defect evolution rather than the ballistic atom collision process.

Acknowledgments

Project supported by the Dean's Fund of China Institute of Atomic Energy (Grant No. 219256) and the CNNC Science Fund for Talented Young Scholars.

References

[1] Dewangan S K, Mangish A, Kumar S, Sharma A, Ahn B and Kumar V 2022 *Eng. Sci. Technol.* **35** 101211
[2] Pickering E J, Carruthers A W, Barron P J, Middleburgh S C, Armstrong D E J and Gandy A S 2021 *Entropy* **23** 98
[3] Li J, Meng X, Wan L and Huang Y 2021 *J. Manuf. Process* **68** 293
[4] Yang T, Li C, Zinkle S J, Zhao S, Bei H and Zhang Y 2018 *J. Mater Res.* **33** 3077
[5] Lu C, Yang T, Jin K, Gao N, Xiu P and Zhang Y 2017 *Acta Mater.* **127** 98
[6] Senkov O N, Gild J and Butler T M 2021 *J. Alloys Compd.* **862** 158003
[7] Zhang Y, Zhao S, Weber W J, Nordlund K, Granberg F and Djurabekova F 2017 *Curr Opin Solid State Mater Sci.* **21** 221
[8] Tsai M and Yeh J 2014 *Mater. Res. Lett.* **2** 107
[9] Hu B, Yao B, Wang J, Liu Y, Wang C and Du Y 2020 *Intermetallics* **118** 106701
[10] Jia N, Li Y, Liu X, Zheng Y, Wang B and Wang J 2019 *JOM* **71** 3490
[11] Yang X, Zhang Y and Liaw P K 2012 *Procedia Eng.* **36** 292
[12] Yin X, Dou Y, He X, Jin K, Wang C and Dong Y G 2023 *Acta Metall Sin.* **36** 405
[13] Yin X, Dou Y, He X, Jin K, Wang C and Dong Y 2022 *JOM* **74** 4326
[14] Lee C, Maresca F, Feng R, Chou Y, Ungar T and Widom M 2021 *Nat. Commun.* **12** 5474
[15] Scales R J, Armstrong D E J, Wilkinson A J and Li B S 2020 *Materialia* **14** 100940
[16] Lee C, Song G, Gao MC, Feng R, Chen P and Brechtl J 2018 *Acta Mater.* **160** 158
[17] Jia N, Li Y, Huang H, Chen S, Li D and Dou Y 2021 *J. Nucl. Mater.* **550** 152937
[18] Mei L, Zhang Q, Dou Y, Fu E G, Li L and Chen S 2023 *Scr. Mater.* **223** 115070
[19] Nordlund K, Zinkle S J, Sand A E, Granberg F, Averback R S and Stoller R E 2018 *J. Nucl. Mater.* **512** 450
[20] Stoller R E 2012 *Compr. Nucl. Mater.* **1** 293
[21] Shi T, Su Z, Li J, Liu C, Yang J and He X 2022 *Acta Mater.* **229** 117806
[22] Zhao S, Xiong Y, Ma S, Zhang J, Xu B and Kai J 2021 *Acta Mater.* **219** 117233
[23] Lin Y, Yang T, Lang L, Shan C, Deng H and Hu W 2020 *Acta Mater.* **196** 133
[24] Deluigi O R, Pasianot R C, Valencia F J, Caro A, Farkas D and Bringa E M 2021 *Acta Mater.* **213** 116951
[25] Zhang Y, Stocks G M, Jin K, Lu C, Bei H and Sales B C 2015 *Nat. Commun.* **6** 8736
[26] Levo E, Granberg F, Fridlund C, Nordlund K and Djurabekova F 2017 *J. Nucl. Mater.* **490** 323
[27] Shan C, Lang L, Yang T, Lin Y, Gao F and Deng H 2020 *Comput. Mater. Sci.* **177** 109555
[28] Granberg F, Nordlund K, Ullah M W, Jin K, Lu C and Bei H 2016 *Phys. Rev. Lett.* **116** 135504
[29] Lu C, Li M, Xiu P, Wang X, Velişa G and Jiang L 2021 *J. Nucl. Mater.* **557** 153316
[30] Li H, Zhao L, Yang Y, Zong H and Ding X 2021 *J. Nucl. Mater.* **555** 153140
[31] Zhang Z, Han E and Xiang C 2021 *J. Mater. Sci. Technol.* **84** 230
[32] Trinkaus H, Singh B N and Foreman A J E 1997 *J. Nucl. Mater.* **249** 91
[33] Wang X, Gao N, Wang Y, Liu H, Shu G and Li C 2019 *J. Nucl. Mater.* **519** 322
[34] Dou Y, Zhao Y, He X, Gao J, Cao J and Yang W 2022 *J. Nucl. Mater.* **573** 154096
[35] Zhao Y, Dou Y, He X, Deng H, Wang L and Yang W 2023 *Comput Mater Sci.* **218** 111943
[36] Plimpton S 1995 *J. Comput. Phys.* **117** 1
[37] Qiu R, Chen Y, Liao X, He X, Yang W and Hu W 2021 *J. Nucl. Mater.* **557** 153231
[38] Stukowski A 2009 *Model Simul. Mat. Sci. Eng.* **18** 015012
[39] Stukowski A 2014 *JOM* **66** 399
[40] Stukowski A 2012 *Model Simul. Mat. Sci. Eng.* **20** 045021
[41] Larsen P M, Schmidt S and Schiøtz J 2016 *Model Simul. Mat. Sci. Eng.* **24** 055007
[42] Li H, Zhao L, Yang y, Zong H and Ding X 2021 *J. Nucl. Mater.* **555** 153140
[43] Jung W D, Schmidt F A and Danielson G C 1977 *Phys. Rev. B* **15** 659
[44] Senkov O N and Miracle D B 2001 *Mater. Res. Bull.* **36** 2183
[45] Zepeda L A, Rottler J, Han S, Ackland G J, Car R and Srolovitz D J 2004 *Phys. Rev. B* **70** 060102
[46] Qiu R, Chen Y, Gao N, He X, Dou Y, Yang W, Hu W and Deng H 2023 *Nucl. Mater. Energy* **34** 101394
[47] Peng Q, Meng, F, Yang Y, Lu C, Deng H, Wang L, De S and Gao F 2018 *Nat. Commun.* **9** 4880